Reviews

Developmental Dynamics
DOI 10.1002/dvdy.24497

Heart Function and Hemodynamics Analysis for Zebrafish Embryos

Huseyin C. Yalcin[1], Armin Amindari[2], Jonathan T. Butcher[3], Asma Althani[1] and Magdi Yacoub[4]

[1]Biomedical Research Center, Qatar University, PO Box 2713, Doha, QATAR

[2]Faculty of Mechanical Engineering, Istanbul Technical University, Istanbul, TURKEY

[3]Department of Biomedical Engineering, Cornell University, Ithaca NY, USA

[4]Imperial College, NHLI, Heart Science Centre, Harefield, Middlesex, UB9 6JH, UK

Address for Correspondence:

Huseyin C. Yalcin, PhD

Assistant Professor of Metabolic Diseases

Biomedical Research Center

Qatar University

Doha, QATAR

Phone: +974 4303 7719

E-mail: hyalcin@qu.edu.qa

Keywords: zebrafish embryo, hemodynamics, blood flow, heart development, shear stress, pressure, mechanobiology, time lapse microscopy, light sheet fluorescent microscopy, particle image velocimetry, computational fluid dynamics

Received: Nov 11, 2016; Revised: Feb 24, 2017; Accepted: Feb 24, 2017

Abstract

The zebrafish has emerged to become a powerful vertebrate animal model for cardiovascular research in recent years. Its advantages include easy genetic manipulation, transparency, small size, low cost, and the ability to survive without active circulation at early stages of development. Sequencing the whole genome and identifying orthologue genes with human genome enabled to induce clinically relevant cardiovascular defects via genetic approaches. Heart function and disturbed hemodynamics need to be assessed in a reliable manner for these disease models in order to reveal mechanobiology of induced defects. This effort requires precise determination of blood flow patterns as well as hemodynamic stress (i.e. wall shear stress and pressure) levels within the developing heart. While traditional approach involves time-lapse brightfield microscopy to track cell and tissue movements, in more recent studies fast light sheet fluorescent microscopes are utilized for that purpose. Integration of more complicated techniques like particle image velocimetry and computational fluid dynamics modeling for hemodynamic analysis holds a great promise to the advancement of the zebrafish studies. Here, we discuss the latest developments in heart function and hemodynamic analysis for zebrafish embryos and conclude with our future perspective on dynamic analysis of zebrafish cardiovascular system.

Introduction

Mouse is the established mammalian model for cardiovascular research. Knock out mouse models enabled to investigate numerous congenital heart defect (CHD) types (Li et al., 2015; Ta-Shma et al., 2016). Embryonic chick is a commonly used vertebrate model with the advantage of resembling human heart structure with four chamber/four valve configuration and enabling clinically relevant surgical manipulations. Embryonic zebrafish has emerged more recently for cardiovascular research to be used in high throughput studies. Even though zebrafish heart is different from human heart with only systemic circulation, heart structure and physiology are similar between two species. Unique characteristics for zebrafish embryos make them particularly attractive for cardiovascular research. For example, there are available practical genetic interference approaches like morpholino injections to induce cardiac defects in zebrafish. These embryos are transparent and can be imaged noninvasively throughout cardiac development. Heart chambers and vessels as well as blood flow can be visualized easily *in vivo*. At early stages of development, zebrafish embryos are not dependent on circulatory system, since passive diffusion is sufficient for oxygen delivery (Pelster and Burggren, 1996). Therefore, embryos having severe heart defects survive early development enabling investigation of mutations for which mammalian models are not appropriate. This way, cardiac valve development in the absence of blood flow was investigated and these studies demonstrated the significant influence of blood flow dynamics on heart valve development (Kalogirou et al., 2014; Steed et al., 2016a).

With the advancement of forward and reverse genetics approaches, it is now possible to induce a variety of clinically relevant cardiac defects in zebrafish embryos. Analysis of blood flow hemodynamics is needed in these animal models for investigating mechanobiological mechanisms of induced defects. There are a variety of microscopic imaging and computational modeling approaches for qualitative and quantitative hemodynamic analysis. These analyses involve determination of flow patterns, measuring flow velocities, calculating heart function parameters, and calculating hemodynamic stress levels. Below, after a brief review of zebrafish heart development and genetic interference approaches, we will discuss these analysis techniques on zebrafish embryos for cardiovascular studies.

Zebrafish heart development

The first organ that forms and starts functioning in vertebrate embryos is the heart. As opposed to bi-ventricular mammalian heart, adult zebrafish heart is composed of one ventricle, one atrium, one atrioventricular (AV) valve and one outflow valve. Genetic pathways are conserved among vertebrate species and zebrafish heart development proceeds through similar steps with other vertebrates. It begins with the specification of pre-cardiac cells as early as 5 hours post-fertilization (hpf) in the anterior lateral plate mesoderm and continues with gastrulation resulting in the formation of ectoderm, endoderm and mesoderm germ layers (Stainier, 2001). Gastrulation is completed at 10 hpf, which is followed by the fusion of bilateral heart fields at the embryonic midline at 16 hpf. This results in the formation of a cardiac cone which then extends anteriorly and transforms into a linear heart tube (Glickman and Yelon, 2002; Poon and Brand, 2013). Outer layer of the linear heart tube is composed of contractile myocytes, whereas inner layer is composed of endocardial cells. The two layers are separated by an acellular extracellular matrix layer known as cardiac jelly. Following its formation, linear heart tube starts to contract in a rhythmic peristaltic manner at 24 hpf. First heart beat starts at 3 weeks in human, at E8.5 in mice and at HH 10 in chicken (Lindsey et al., 2014). Degree of contractility in zebrafish embryos for subsequent stages can be quantified using high-speed time lapse video microscopy to determine ventricular fractional shortening, which is a comparison of ventricular dimensions at diastole and systole (Houk and Yelon, 2016). Even though there are no valves present at this stage, blood is pumped out at 250 µm/s peak velocity without significant backflow (Goetz et al., 2014; Boselli et al., 2015). Shortly later, lumen starts to open and stroke volume as well as heart beat rises quickly. At 28 hpf, heart beat is regular at 2.6 Hz (Boselli et al., 2015). Heart tube undergoes a leftward looping into an S-shape at 33 hpf, which displaces the ventricle into the right of the atrium. At 36 hpf, pumping mechanisms transits from slow peristaltic waves into sequential chamber contractions suggesting the onset of cardiac conduction system. By 2 days post-fertilization (dpf), ventricular chamber balloons out with distinct outer and inner curvatures. At this stage, cardiomyocytes start delaminating from the ventricle wall to start trabeculation, and by 72 hpf ventricle has obvious trabecular ridges (Liu et al., 2010). Trabecular myocardium expands towards the ventricular cavity as the cardiac wall undergoes significant remodeling along with the compact myocardium proliferation and maturation of the conduction system (Samsa et al., 2013; Brown et al., 2016). Genetics screening studies revealed molecular regulation of these early events in zebrafish. GATA factors in association with Nkx2.5 were shown to control cardiomyocyte progenitor migration and regulation of cardiac fate specification by restriction of Wnt signaling (Kuo et al., 1997; Lu et al., 2016). Hand2 plays role in cardiac differentiation and morphogenesis (Trinh et al., 2005; Garavito-Aguilar et al., 2010) whereas Nkx2.5 maintains cardiac chamber identity (Targoff et al., 2008; Targoff et al., 2013). More recently, cardiac contraction and resulting fluid forces were shown to activate Notch signaling to modulate cardiac trabeculation in zebrafish (Samsa et al., 2015; Lee et al., 2016b).

Heart valves composed of leaflets ensure unidirectional blood flow in zebrafish. There is one valve in the AV canal between atrium and ventricle and one valve in the outflow tract between ventricle and bulbus arteriosus. AV valve development starts with the myocardial expression of bmp4, tbx2b, and vcana and endocardial expression of notch1b, has2 and neuregulin at 37 hpf (Poon and Brand, 2013). Hemodynamic forces are important mechanical stimuli for AV valve development in zebrafish. For example, klf2a expression were shown to be dependent on the presence of reversing flows (Vermot et al., 2009) whereas shear stress governs differential expression of miR-21 in AV canal (Banjo et al., 2013). At 40 hpf, endocardial cushions start to transform into primitive valve leaflets (Beis et al., 2005; Martin and Bartman, 2009). The presence of epithelial-to-mesenchymal transition for zebrafish valvulogenesis has been debated but not confirmed yet (Pestel et al., 2016; Steed et al., 2016b). Endocardial cushions remodel into primitive valve leaflets to prevent retrograde flow completely at 76 hpf (Scherz et al., 2008). Blood velocity through endocardial cushions at this stage is at about 3.0 mm/s peak velocity with max wall shear stress (WSS) level of 70 dynes/cm^2 (Hove et al., 2003). Formation of endocardial cushions occurs at 4.5 weeks in human, at E12 in mice and at HH24 in chicken (Lindsey et al., 2014). There are four cusps in zebrafish AV valve (Hu et al., 2001). In the outflow tract, bulbous arteriosus is composed of a thick outer layer with smooth muscle cells and a thin inner layer with endothelial cells. This small chamber is elastic and ensures preservation of high pressures to prevent backflow from the aorta. The outflow valve has only two leaflets as opposed to three leaflet mammalian aortic valve. Zebrafish heart development is summarized in Figure 1.

Flow through primitive zebrafish heart can be measured by simply tracking individual erythrocytes. Alternatively, for more detailed flow analysis, digital particle image velocimetry

(DPIV) can generate spatial flow maps through correlations of particle locations (in most case fluorescing eryhthrocytes) between sequential frames (Jamison et al., 2013). Both of these techniques require fast image acquisition of at least 150 frames per second (fps). Either erythrocytes or blood plasma should be fluorescently labeled for enhanced contrast. A different approach which was recently introduced is to computationally estimate the flow field based on deformations of the myocardial walls (Boselli and Vermot, 2016). DPIV and computational modeling identified oscillatory flow regimes within zebrafish hearts which were shown to be critical for regulating gene expressions for valve development (Hove, 2006; Heckel et al., 2015).

Genetic approaches in zebrafish

While embryonic chick is widely used in surgical/mechanical interference studies (Yalcin et al., 2010a; Yalcin et al., 2010b; Yalcin, 2014; Gould et al., 2016), zebrafish embryos are suitable for genetic interference. Zebrafish genome sequence is known and forward/reverse genetic approaches were successfully applied on zebrafish embryos to identify molecular pathways for studying function of specific genes. Forward genetics is determining the genetic basis leading to a specific phenotype for an organism. Reverse genetics on the other hand is to selectively manipulate a previously identified gene and analyze the impact of this manipulation on the organism (Bournele and Beis, 2016). For zebrafish, forward genetics based random mutations were successfully induced via radiation or chemical treatment and stable lines were generated for incrossed generations (Chico et al., 2008). Hundreds of mutants with abnormal cardiovascular development were generated with this approach (Chen et al., 1996). For example, several mutations leading to valve defects and aortic coarctation were identified by forward genetics screening (Weinstein et al., 1995; Stainier et al., 1996). Another example for forward genetics is the double mutant line, casper. This mutant does not have melanocytes and iridophores, which makes it transparent through its life enabling non-invasive imaging (White et al., 2008).

Several reverse genetic techniques are available as well for zebrafish embryos to selectively knock down gene function. The most commonly utilized technique is injecting antisense morpholino oligonucleotides (MOs) into the fertilized egg. MOs can inhibit translation by targeting transcriptional start site, or by targeting splice junctions and inducing abnormal splicing. Protein synthesis for the targeted gene(s) is effectively prevented for 3-5 days (Nasevicius and Ekker, 2000). Due to easy utilization in zebrafish, MOs have enabled widespread analysis of gene function. It quickly became apparent that some MOs work very well, and there are many MO phenotypes that effectively recapitulate mutant phenotypes without any major side effects. However, MOs can induce p53-dependent apoptosis and off-target cell specific effects in gene expression that might compromises phenotypic analysis (Kok et al., 2015). In a large collection of knockout lines, nearly 80% of MO morphant phenotypes failed to be observed in the corresponding mutants, leading to questioning widespread utilization of MOs in zebrafish research (Lawson, 2016). It has been suggested that MOs should not be injected in excessive amounts to limit off-target effects and stable mutants must be generated and appropriately characterized to validate MO morphant phenotypes (Rossi et al., 2015). Two alternative techniques for reverse genetics have been recently introduced for zebrafish: TALENs and Crispr/Cas9 (Schulte-Merker and Stainier, 2014). These techniques affect genomic DNA, rather than RNA transcripts. Therefore, their molecular effects can be determined at the single embryo level (which is more difficult with MOs) to obtain a clear phenotype/genotype correlation. Off-target effects of these techniques were shown to be negligible (Stainier et al., 2015).

These genetic approaches were used to generate human cardiovascular diseases on zebrafish embryos to uncover molecular mechanisms. One widely investigated condition is cardiomyopathy. Cardiomyopathy is the disease of heart muscle. There are two prevalent forms: dilated cardiomyopathy and hypertrophic cardiomyopathy. Forward genetic screening of zebrafish mutants with cardiomyopathy revealed that mutation in titin, laminin alpha4 and integrin-linked kinase result in heart failure mimicking human clinical condition. In a reverse genetic study, after identification of EYA4 mutations for human patients with DCM, EYA4 gene in zebrafish was knocked down via morpholino injection. Resulting phenotype possessed cardiomyopathy demonstrating the role of EYA4 mutation on the condition (Chico et al., 2008). Our group has identified several mutations in myosin binding protein C in hypertrophic cardiomyopathy patients and recapitulated these mutations in the zebrafish model via morpholino injections (unpublished data). Heart function analysis and hemodynamics assessment are important in these and similar animal defect models. Below, we explain these analysis techniques for zebrafish embryos.

Heart function analysis from brightfield time-lapse image sequences

At early stages of zebrafish development (3-4 dpf), the embryos are transparent with good visibility of internal organs including heart and blood circulation. Therefore, video brightfield microscopy can be used for quantification of heart function and morphology at this stage. Approach is based on recording 2D image sequences for further cardiovascular analysis. For this purpose, the animal is positioned in a lateral position with the ventricle clearly visible throughout the full cardiac cycle. In this configuration, atrium is not visible (Figure 2A, B). Myocardial wall velocity can be measured for ventricular function using automated video edge detection systems (Denvir et al., 2008). 120 frame per second (fps) video capturing speed is sufficient for this application. Systolic wall velocity levels were measured as about 200 µm/s at 2dpf and about 275 µm/s at 6 dpf embryos. Ventricular wall motion can also be practically analyzed with an approach analogous to M-mode echocardiography. The aim here is to follow continuous changes in ventricular wall position throughout cardiac cycle. This can be done by first identifying a linear region of interest. This region would be either short axis or long axis of the ventricle. The pixel intensity of every point in this line can be measured in all the recorded images of the cardiac cycle (Shin et al., 2010) (Figure 2B). For the M-mode image, the intensity values along this line is Y axis and each frame of the video is represented in the X axis. This way, changes in ventricular short axis and long axis diameters can be measured throughout cardiac cycle. M-mode analysis enables to track myocardial wall thickness and ventricle diameter. Short axis diameters for diastole and systole are represented as D_d and D_s and myocardial thicknesses are represented as MT_d and MT_s in Figure 2B. Images should be captures at 250 fps for good temporal resolution for this application.

Blood flow velocities are measured to quantify cardiovascular function for zebrafish embryos. This can be achieved by simply tracking movements of red blood cells (RBCs) in the embryo`s body, which are easily identifiable due to transparent skin (Shin et al., 2010) (Figure 2C). Acceleration, deceleration, and peak velocity for RBC movements (hence for blood flow) can be calculated for analysis. RBC movements in two main vessels through the body, in dorsal aorta and in cardinal vein can be imaged for this purpose. Location of individual cells are determined from sequential frames and RBC velocity is calculated from coordinates of the location of the cell and time interval between the frames as follows:

$$RBC\ velocity = \frac{\sqrt{(x_2 - x_1)^2 - (y_2 - y_1)^2}}{\Delta t}$$

Mean RBC velocity in dorsal aorta were shown to increase from 291 µm/s at 2 dpf to 766 µm/s at 6dpf (Bagatto and Burggren, 2006).

Structural analysis of the zebrafish hearts is based on taking 2D images at specific timepoints to measure chamber dimensions. For example measurement of myocardial thickness is essential to assess severity of induced defect for hypertrophic cardiomyopathy condition (Figure 2D). Fractional area change (FAC) is an established parameter for ventricular function to evaluate contractility in zebrafish embryos (Haendchen et al., 1983). It can be calculated from analyzing 2D still frames of ventricle at end-diastole (ED) and end-systole (ES) (Figure 2D). ED is the fully dilated ventricle and ES is the fully contracted ventricle. Ventricular areas (EDA and ESA) are calculated at these two points and FAC is calculated as follows:

$$FAC = 100\ \times \frac{(EDA - ESA)}{EDA}$$

Fractional shortening (FS), another measure of ventricular contractility can be calculated from ventricular diameters at end diastole and end systole (D_d and D_s) as follows (Shin et al., 2010):

$$FS = \frac{(\ D_d - D_s)}{D_d}$$

Ventricular volumes need to be calculated for evaluating stroke volume, ejection fraction and cardiac output. This is done by first measuring long and short axis diameters (D_L and D_S) from 2D still images. By assuming a prolate spheroidal shape for the ventricle, following volume formula can be used:

$$Volume = \frac{1}{6} \times \pi \times D_L \times {D_S}^2$$

Stroke volume (SV) is the blood volume pumped from the ventricle for each beat and is simply calculated from ventricle volumes at end-diastole (EDV) and end-systole (ESV) (DeGroff, 2002) :

$$SV = (EDV - ESV)$$

SV was found to increase from 0.146 nanoliter at 2 dpf to 0.297 nanoliter at 6dpf (Bagatto and Burggren, 2006).

Ejection fraction (EF) is defined as the fraction of blood ejected from the ventricle with each heart beat and can be calculated from the following formula:

$$EF\ (\%) = \frac{(EDV - ESV)}{EDV} \times 100 = \frac{SV}{EDV} \times 100$$

Cardiac output (CO) can be calculated from SV and heart rate (HR):

$$CO\ (nanoliter/min) = SV\ (nanoliter/beat) \times HR\ (beats/min)$$

HR is simply determined by measuring the time between two identical successive points (i.e. ED or ES) in the recorded images (Hoage et al., 2012). CO was found to increase from 9.3 nanoliter/min at 2 dpf to 55.6 nanoliter/min at 6dpf (Bagatto and Burggren, 2006).

A protocol explaining functional analysis for zebrafish hearts is provided as a supplemental material. See supplemental movie 1 for ventricular wall movements and supplemental movie 2 for RBC movements for a 3dpf embryo.

Abovementioned 2D cell and tissue tracking techniques usually require high frame rate imaging (~250 fps) systems and automated image analysis algorithms. Several groups use custom made systems (Shin et al., 2010; Liu et al., 2014) . Manual cell tracking protocols are available as well (Hoage et al., 2012). There are also a number of software that can be used for that purpose. SOHA is a free example application (Fink et al., 2009; Cammarato et al., 2015).

Calculation of ventricular volumes from 2D length measurements involves errors because of the heart`s irregular shape and asymmetry (as opposed to symmetric prolate spheroid shape assumption). Therefore calculating stroke volume, ejection fraction and cardiac output based on 2D measurements does not allow precise results. Generating 3D ventricular volumes by combining 2D images from different angles resulted in a better representation for the shape of the heart. CO calculated from more accurate 3D shapes were about 10% higher than the 2D method values (Bagatto and Burggren, 2006). Therefore, 2D volume calculation method should be utilized with caution especially with disease models having significant irregular shapes. Integration of confocal or micro-CT based 3D volume generation methods will enhance accuracy for these measurements. We have previously established a micro-CT based technique for 3D cardiac geometry generation for fixed chicken embryos (Butcher et al., 2007; Yalcin et al., 2011). We then extended the work by limiting radiation exposure to image live chicken embryos (Henning et al., 2011). Integration of these approaches to embryonic zebrafish studies will enhance accuracy for volume measurements. Ultrasound biomicroscopy is another imaging technique which has provided useful information for adult zebrafish cardiovascular function (Lee et al., 2016b; Nair et al., 2016; Wang et al., 2016). The development of higher frequency probes (>100MHz) is expected to enable embryonic zebrafish imaging using this technique in the near future.

3D live imaging via light sheet fluorescent microscopy

Zebrafish embryos have been used for decades now for developmental biology research. High resolution imaging for zebrafish embryonic hearts is very demanding due to the fast heart rate of 2-4 hz and the relatively large size of about 250 µm. Therefore, in-vivo functional and structural imaging for the zebrafish cardiovascular system requires an advanced microscope that can record optical sections at high temporal and spatial resolution. Conventional confocal laser-scanning fluorescence microscopy (CLSM) is based on point scanning of the object. Therefore, the technique is naturally slow and causes high photo-bleaching/photo-toxicity because of the non-selective excitation with high laser powers. The depth penetration is also relatively low, therefore it is challenging to capture beating zebrafish embryonic hearts especially for older embryos. Light sheet fluorescence microscopy (LSFM) was introduced in 2004 to eliminate the limitations of CLSM (Huisken et al., 2004). The technique is known as selective plane illumination microscopy (SPIM). The working principle is based on illumination of a fluorescently labeled specimen from the side with a thin laser sheet, excitation of the fluorescence only in the focal plane of the detection objective, and simultaneous recording of the emission light (Weber and Huisken, 2011) (Figure 3A). The detection system in LSFM includes CCD/sCMOS cameras rather than a scanning photomultiplier tube detector as in CLSM. Therefore, LSFM provides several important advantages including improved acquisition speeds, high signal-to-noise ratio, low photo bleaching and large penetration depths (Huisken and Stainier, 2009) (Figure 3B). Additionally, in most applications, sample is housed in a dedicated vertical mount (a transparent syringe or a capillary) and is immersed into a medium-filled imaging chamber. The sample is embedded into low concentration agarose cylinders, which represents a less stressful environment for live biological samples than traditional glass slides (Tomer et al., 2011). Vertical mounting also enables rotating the delicate samples without deforming them and facilitates 360° imaging. Therefore, LSFM became the new standard imaging modality for zebrafish studies, since it enables fast and high-resolution dynamic imaging within a physiological imaging medium.

LSFM enhanced cardiac function analysis for zebrafish embryos significantly. Specific regions inside the heart can now be imaged *in vivo* at high resolutions. These high-speed movies from a single plane can be used to calculate many parameters to describe heart function. Figure 4A shows AV canal for a 60 hpf embryo for which myocardial cells are labeled green and RBCs are labeled red (Lee et al., 2016a). Myocardial wall deformations and RBC movements can be tracked for this configuration at the selected plane. However, for a complete and accurate functional analysis of the heart, 3D analysis is needed on 3D reconstructed beating heart images. The constant and fast movements of the heart in all dimensions make it very difficult to capture such high-resolution images. One solution is to suppress the heart as in the silent heart model (Chi et al., 2010). However, this model is not applicable to investigate the hemodynamics and cardiac contraction during heart development. An alternative method is obtaining a still 3D heart using prospective gating techniques. Here, while the heart continues to beat, it is slowly moved in small steps through the focal plane of the imaging objective. At each plane, a fluorescent image is taken for a predefined phase in the cardiac cycle. These images are then 3D reconstructed to generate a model of the heart at this specific phase (Taylor et al., 2012a; Taylor et al., 2012b; Weber and Huisken, 2015). However, dynamics of the heart beat cannot be studied this way. Dynamics of a beating heart can be fully analyzed only via 4D imaging (3D+time), which requires extremely fast image acquisition and depth penetration. Advancement in post-acquisition synchronization techniques enabled to capture the dynamics of zebrafish embryonic beating hearts in 4D. In this technique, retrospective temporal registration of image stacks enables to reconstruct the dynamic motion of cardiac tissues (Liebling et al., 2006). At successive optical sections for entire depth of the heart, short movies of the beating heart are recorded. Image sequences from consecutive z-planes are then retrospectively registered in time to produce a 4D movie of the beating heart (Mickoleit et al., 2014; Trivedi et al., 2015). Pericardial cells, myocardial cells and RBCs can be fluorescently stained, and 3D movies recorded at 70-85 fps can be used to make 4D movies enabling detailed and dynamic heart function analysis (Trivedi et al., 2015; Weber and Huisken, 2015; Lee et al., 2016a) (Figure 4B). More recently, integration of two photon excitation to LSFM resulted in enhancement of penetration depth and preservation of light sheet thickness enabling high acquisition speed (>70 fps) and low photodamage (Truong et al., 2011). Recent approaches have been developed for further advancing scanning speeds. One is multicolor LSFM. Mahou et.al. implemented mixed-wavelength excitation to achieve fast multi-color two photon imaging (Mahou et al., 2014). This way, they could simultaneously image CFP, GFP and DsRed labeled pericardial, myocardial and RBCs respectively. Fast time series images were acquired at 85 fps, which were then used to generate 4D movies for heart`s periodic motion. The technique did not produce additional photodamage compared to one color LSFM. Simultaneous imaging of myocardial, and RBCs resulted in improved dynamic analysis (Mahou et al., 2014). Finally, advances in image acquisition enabled the direct recording of 4D movies for beating hearts (Figure 4C). Here, a tunable electric lens was used as a remote focusing system and synchronization of this system with the scan mirror of LSFM resulted in the elimination of moving the sample or any other microscope component. The modification enabled to reach scanning speeds way beyond conventional volumetric imaging modalities (Fahrbach et al., 2013). The entire heart could be instantaneously recorded in rapid sequence. This high-speed microscope was used to deliver 3D snapshots of a beating zebrafish heart imaged from 17 planes at 510 fps equivalent to 30 volume scans per second.

Light sheet microscopes can now record dynamic motion of the myocardial walls and RBCs and this advancement resulted in the application of advanced techniques like particle image velocimetry and computational modeling to zebrafish cardiovascular hemodynamic analysis. In the next sections, these advanced techniques are explained.

Shear stress analysis via digital particle image velocimetry (DPIV)

Wall shear stress (WSS) is the frictional force in the cardiovascular system acting on the blood vessel walls and valve leaflet surfaces. It is the product of shear rate (velocity derivative with respect to vessel radius) and dynamic viscosity of blood (i.e. viscosity of a fluid is a measure of its resistance to gradual deformation by stress). Quantitative and qualitative analysis of WSS in the cardiovascular system is important since both its magnitude and orientation are thought to contribute to cardiogenesis. There is significant evidence suggesting that, WSS on cardiovascular endothelial cells can substantially influence vascular and valvular development as well as pathogenesis of vascular and valvular disease in adult organisms (Langille, 1995; Hove, 2006; Buskohl et al., 2012). Flows with different fluid mechanics characteristics (i.e. steady vs. unsteady, laminar vs. turbulent, anterograde vs. oscillatory) were shown to differentially regulate specific gene expression pathways in endothelial cells (Braddock et al., 1998; Barbee, 2002; Lieu et al., 2004). Therefore accurate determination of shear stress patterns and shear stress levels are significantly important for clinical as well as for in-vivo studies on cardiovascular diseases. *In vivo* mapping of the WSS in the cardiovascular system is extremely difficult. Since WSS is directly proportional to axial velocity gradient at the vessel wall, velocity gradient at that location should be determined to calculate WSS. However, this is not an easy task for several reasons: complex geometry, unsteady pulsed flow behavior, moving boundaries (i.e. blood vessel walls and valve leaflets), and Non-Newtonian behavior of blood (i.e. viscosity of blood changes with shear rate, shear thinning characteristics). Therefore, simplifying assumptions like ideal geometries, steady flow, simple parabolic velocity profile, Newtonian behavior etc. for WSS calculations are usually adapted but these lead to unreliable results. DPIV has emerged as a powerful tool to determine velocity vectors and WSS levels in the cardiovascular system for in-vivo studies. The technique has been used since 1970s for general flow studies and in the last 15-20 years, it has been adapted to biological research. DPIV is based on tracking reflective particles in a flow. Once appropriate particles are selected and added to flow, these particles will move with the flow velocities. Two consecutive images of these particles are acquired at a short time interval using a high-speed camera. Displacement vectors for each particle are obtained from these images and this information is then used to determine velocity vectors for the particles (hence for the flow field). For studies involving large geometries (like the flow around an automobile), small reflective particles are seeded in the fluid and these are illuminated as they pass through a laser sheet. For small geometries like zebrafish cardiovascular flow, DPIV requires microscopic analysis of the flow fields. Here the diameter of tracer particles is critically important such that, these should be large enough to be individually identified and at the same time small enough to follow local flows.

For DPIV of zebrafish blood flow, either erythrocytes or injected beads can be tracked. In the pioneering study by Hove et.al., velocity and WSS levels were determined by tracking erythrocytes. At 37 hpf, peak velocities in AV canal were 0.9 mm/s and in outflow tract 1.5

mm/s corresponding to peak WSS of 2.5 – 10 dynes/cm^2. Peak WSS in AV canal were calculated as 76 dynes/cm^2 at 4.5 dpf (Hove et al., 2003). For enhanced accuracy for DPIV, cells can be fluorescently labeled or alternatively, injected fluorescent particles can be tracked (Hove, 2006). A recent study compared the accuracy of flow measurements with tracking RBCs and tracer particles and found out that, at high magnification (25X), tracing RBCs results in significant errors by underestimating velocities. At medium magnification (12.5X), there is no difference in using RBCs or particles as tracers (Poelma et al., 2012). Identification of vessel wall locations is critically important for DPIV analysis. Inner surface of the vessel walls are not directly identified. Instead, locations of the tracer particle limits are identified via computer algorithms.

DPIV can be done in either 2D planes or 3D volumes. Jamison et.al. captured brightfield image series of RBCs for 3dpf to 6dpf embryos at 2000fps. 2D velocity vector maps were determined for ventricular flows (Jamison et al., 2013) (Figure 5). They found that, while the maximum velocity at the outflow valve was around 3 mm/s at 3dpf, it gradually decreases to lower values for older embryos since outflow valve expands as the embryo grows. As a result, max wall shear rate at the outflow valve at peak systole was about 440 s^{-1} for 3 dpf embryos which corresponds to about 31 dynes/cm2 (with dynamic viscosity assumption of 0.07 dynes s/cm^2) and decreases gradually to about 180 s^{-1} at 6 dpf which corresponds to about 13 dynes/cm^2. In contrary to outflow valve, peak AV canal velocities were shown to increase as the embryo develops: ~0.8 mm/s at 30 hpf, ~3.5 mm/s at 70 hpf and ~5 mm/s at 120 hpf (Lee et al., 2013). Tracing injected fluorescent particles instead of RBCs facilitates image acquisition due to better control of particle size and density. As a rule of thumb, frame capturing speed should be at least ten times the heart rate of the embryos, 30fps for 3hz heartbeat. Higher capturing speeds are necessary for older embryos because of higher blood velocities (Hove and Craig, 2012). 0.2µm

- 1µm fluorescent beads are appropriate for 3dpf – 6dpf embryos (Hove and Craig, 2012). Appropriate concentrations should be determined for preventing bleeding and interference with normal cardiac physiology (Goktas et al., 2015). For DPIV analysis, tracking software such as Image J, Improvision Volocity or Metamorph are generally used (Hove and Craig, 2012). More recently, 3D DPIV for obtaining 3D velocity fields became possible by the introduction of high-speed light sheet fluorescent systems. For example, a conventional light sheet fluorescent microscope with confocal platform can scan about 240 image planes in each second which corresponds to generating thirty 8-plane z-stacks in one second (at moderate resolution of 256 x 512), which is suitable for 3D imaging of 3-4dpf zebrafish hearts with 3 hz heart beat (Hove and Craig, 2012).

Hemodynamics analysis via computational fluid dynamics (CFD):

CFD modeling is very beneficial in cardiovascular research to investigate complex fluid behavior for which experimental measurements would provide only limited information. For this technique, first an accurate representation of the problem geometry is generated. The second step is defining the conditions in the model boundaries. The third step is dividing zones into smaller elements (meshing), and the last step is numerically solving appropriate governing fluid flow equations in each small element to obtain a solution field of interest (i.e. velocity vectors, WSS, pressure etc.) within the entire geometry. The technique has gained significant attention in the last years to investigate the influence of disturbed hemodynamics on cardiovascular diseases (Caiazzo et al., 2015; Nguyen et al., 2015; Doost et al., 2016). These patient-specific models contributed to the clinical decision making of physicians. CFD modeling has also been used for *in vivo* studies aiming to investigate hemodynamics in a developing heart. Embryonic chick model has been used widely for this purpose. Our group and others have documented characteristics of evolving hemodynamics environment for cardiogenesis of this species (Wang et al., 2009; Yalcin et al., 2011; Bharadwaj et al., 2012; Lindsey et al., 2015). Zebrafish is another animal model that is used very common for cardiovascular research. Previous studies have shown that, similar to other animal systems, mechanical signals contribute to zebrafish heart development. More specifically, fluid shear stress and transmural pressure were shown to affect vascular, chamber and valve morphogenesis through triggering mechano-biological mechanisms within endothelial cells (Hu et al., 2001; Peshkovsky et al., 2011). Disturbing blood flow through a developing heart resulted in altered heart development similar to human CHDs (Hove et al., 2003).

However, interestingly, there is scarcity of CFD studies for detailed hemodynamics investigation on zebrafish model in the literature. In one study, a 2D CFD model was developed for a simplified heart geometry approximating 4.5 dpf zebrafish heart (Miller, 2011). The model is a linear channel with two staggered chambers bulged from opposite sides of the channel, representing atrium and ventricle (Figure 6). Endocardial cushions exist on the dorsal and ventral sides of the inflow tract, AV canal and the outflow tract. Blood flow simulations were executed in two different ways: in the first approach, velocity inlet condition (steady, parabolic velocity profile) is defined in the inlet boundary through a rigid geometry; in the second approach, atrium and ventricle were defined as elastic materials and the flow was enforced by the contracting atrium, which elastically stretches the ventricle (Figure 6A). In both cases, governing fluid flow equations (Navier-Stokes and Continuity) were solved to obtain velocity streamlines patterns and WSS values acting on the walls and endocardial cushions. Analysis of streamline patterns suggested that, moving boundaries should be considered to capture the flow patterns accurately

(Figure 4B). In the rigid model, maximum normal stress was 0.02 dynes/cm^2 on chamber walls and maximum WSS was 2 dynes/cm^2 on endocardial cushions. Simulations with different endocardial cushion heights revealed that the development of these cushions significantly influences WSS distribution and magnitude within the heart as well as the levels of the pressure on chamber walls. Highest WSS is on the cushions and as the height increases, WSS also increases (Figure 4C). Normal pressure force on the walls of the chambers also increases significantly with increased cushion heights due to higher resistance to flow through narrow AV canal. In the elastic model, for the highest cushion case (i.e. the endocardial cushions occupying more than half of the AV canal width), maximum WSS is about 70 dynes/cm^2 which is in agreement with Hove et.al. who calculated WSS for 4.5 dpf embryos as 76 dynes/cm^2 (Hove et al., 2003). Maximum normal force on the chamber walls for the highest cushion height case was 3.5 dynes/cm^2.

In a following study, moving boundary modeling approach on zebrafish hemodynamics was applied to CFD models based on real geometries (Lee et al., 2013). In this study, transgenic zebrafish embryos with GFP labeled endothelial/endocardial cells and gata-1 labeled RBCs were used. GFP labeling enabled to track boundaries of the lumen walls whereas gata-1 labeling enabled to track blood flow (via DPIV) hence measuring blood velocities. Zebrafish embryos at stages 20-30 hpf to 110-120 hpf were included in the study. 2D images of the embryo hearts at 20 fps were collected using a fluorescent microscope. In each image, lumen boundaries were determined by tracking fluorescent endothelial cells (Figure 7A). To generate a moving boundary computational model, for each image, fixed number of mesh nodes were generated in the endocardial wall segmentation. The node movements in the segmentations were then interpolated to enhance temporal resolution. Two-dimensional triangular meshes were generated and based on the wall motion specified by the segmentations throughout the cardiac cycle, meshes were forced to deform during the CFD simulation. DPIV measured velocity profiles at the inlet region of the geometry was used as transient velocity boundary condition in the simulations for different stage models. Models were validated by comparing model velocity results with DPIV measured values at AV canal. Maximum velocities were found to be localized at the AV canal, with levels of ~1 mm/s at 30hpf, ~3.5 mm/s at 70 hpf and ~5 mm/s at 120 hpf (Figure 7B). The results showed that, average WSS levels at AV canal at peak atrial systole were ~3.5 dynes/cm^2 for 20-30 hpf, ~20 dynes/cm^2 for 40-50 hpf and ~80 dynes/cm^2 for 110-120 hpf. Similarly, AV transvalvular pressure gradient increases significantly throughout development. Transvalvular pressures were ~0.3 dynes/cm^2 for 20-30 hpf, ~0.35 dynes/cm^2 for 40-50 hpf, and ~2.5 dynes/cm^2 for 110-120 hpf (Figure 7C). Formation of vortices at different locations for different stage embryos were observed (Figure 7D) suggesting flow patterns might also affect cardiogenesis via mechano-biological signaling.

More recently, a practical approach was developed to estimate WSS levels in a zebrafish heart. The method integrates live confocal imaging with CFD and is based on estimating WSS levels from heart wall dynamics (as opposed to direct determination from RBC movements) (Boselli and Vermot, 2016). In this study, 48 hpf zebrafish embryos were used. Live imaging of Gata1-DsRed labeled RBCs were performed at 120 fps to generate 4D heart views. Maximum projection of the synchronized z-stack gave the 2D representation of the heart volume (Figure 8A). On this 2D geometry, a hydrodynamic centerline was then defined which provided a 1D parametrization of heart anatomy (Figure 8B). Cross sections of the heart were defined by the intersection of segments perpendicular to the walls and the centerline. The wall dynamics were then defined as a function of the wall velocities and the arch length positions within the centerline. These wall velocity estimates were then prescribed as boundary conditions for an *in silico* computational model that allows to calculate blood velocity and WSS values within the geometry (Figure 8C). Peak endocardial WSS was found around 70 dynes/cm^2 (7 Pa) which is consistent with other measurements. The proposed method provides a powerful practical methodology for future zebrafish studies. This methodology was adapted and validated in a recent study on zebrafish heart valve development. The computational model successfully identified oscillatory WSS regimes and authors found that those stress patterns modulates klf2a expression through trpv4 and trpp2 (Heckel et al., 2015).

These works demonstrate the importance of CFD in zebrafish hemodynamics analysis but much more work is needed for better understanding the mechanics of heart development. Computer models need to be developed in 3D and must incorporate, both wall dynamics, and fluid dynamics (fluid-structure interaction approach) for accurate analysis. Molecular regulatory networks responsible for heart development should be studied in parallel experiments for understanding mechanisms of mechanotransduction. One way for this investigation is to find out if the gene expression patterns for heart morphogenesis are controlled either temporally or spatially with induced fluid shear and transmural pressure during heart development. Recent advances in computational modeling techniques now enable studying these complex problems, and are expected to contribute to this field significantly in the near future.

Conclusions and future directions

Over the last decades, zebrafish model has evolved as a very powerful model to study cardiac development. Advances in forward and reverse genetic interference techniques enabled to induce human cardiovascular defects in those animals. Cardiovascular dynamics has been studied in these disease models most commonly via basic 2D brightfield microscopy analyses that involves errors in heart function calculations. Light sheet fluorescent microscopes were developed specifically to image zebrafish embryos. These microscopes enabled to track myocardial wall and RBC movements in real time. Therefore, it is now possible to generate 4D movies of a beating zebrafish heart using these microscopes. However, this approach requires extensive post-acquisition efforts on image registration. Some groups have developed their own algorithms for this purpose but these are not readily applicable to other researchers. Commercialization of such software will be beneficial to numerous research groups working with zebrafish. Recent advancements in image acquisition optics for light sheet microscopes are promising to directly record 4D zebrafish heart movies which will have dramatic contribution to the field. Fast image acquisition via LSFM made it possible to apply advanced techniques like DPIV and computational modeling to zebrafish studies. However, most of the current studies involve hemodynamics analyses in 2D cardiac planes due to imaging and modeling difficulties of small size and fast moving boundaries for the zebrafish heart. Development of 3D micro DPIV systems with working principle of simultaneous image acquisition from different planes will contribute to direct and fast flow visualization of zebrafish hearts in 3D. Even though commercial 3D DPIV systems are available, these cannot image micro sized samples as zebrafish hearts. Ultrasound biomicroscopy and optical coherence tomography systems were utilized successfully for other embryonic animal systems as well as for adult zebrafish. These are potentially very useful modalities for embryonic zebrafish imaging. Current commercial systems are not appropriate for zebrafish embryos due to very small size. We expect development of new probes to image embryonic zebrafish in the near future. As per the CFD modeling, future models should be based on fluid-structure interaction approach to incorporate both wall dynamics and blood flow dynamics. Such 3D models will lead to accurate hemodynamics analysis. Other than genetic approaches, micro surgical approaches should also be developed for zebrafish cardiogenesis. The only such surgical work was the pioneering work by Hove et. al. , where micro beads were inserted in zebrafish hearts to disturb hemodynamics (Hove et al., 2003). Better controlled surgical approaches are needed in zebrafish. Because of the small size, ligation based surgical approaches on embryonic chick are not applicable. Our group has developed a minimally invasive femtosecond laser photoablation technique for embryonic chicken cardiogenesis and were successfully induced micro-defects in atrioventricular valve, vitelline vessels and arch arteries (Yalcin et al., 2010a; Yalcin, 2014; Lindsey et al., 2015). Integration of such techniques to generate zebrafish defect models will open new horizons for the researchers.

Acknowledgements

We would like to thank to Qatar University Biomedical Research Center team for the study; Dr. Asma Alhani, Dr. Gheeyath Nasrallah, Ms. Sahar IsaDas, Dr. Hany Mady, Dr. Hadi Yassine, Dr. Nahla Eltai for scientific support and Ms. Naiema Al-Meer, Ms. Maria Khalid Smatti, and Ms. Fadheela Mohammad for administrative support. This research was supported by Qatar University internal grants (QUST-BRC-SPR\2017-1 and QUUG-BRC-2017-3 to HCY).

Conflict of Interest

None

References

Bagatto B, Burggren W. 2006. A three-dimensional functional assessment of heart and vessel development in the larva of the zebrafish (Danio rerio). Physiol Biochem Zool 79:194-201.

Banjo T, Grajcarek J, Yoshino D, Osada H, Miyasaka KY, Kida YS, Ueki Y, Nagayama K, Kawakami K, Matsumoto T, Sato M, Ogura T. 2013. Haemodynamically dependent valvulogenesis of zebrafish heart is mediated by flow-dependent expression of miR-21. Nature Communications 4:1978.

Barbee KA. 2002. Role of Subcellular Shear–Stress Distributions in Endothelial Cell Mechanotransduction. Annals of Biomedical Engineering 30:472-482.

Beis D, Bartman T, Jin SW, Scott IC, D'Amico LA, Ober EA, Verkade H, Frantsve J, Field HA, Wehman A, Baier H, Tallafuss A, Bally-Cuif L, Chen JN, Stainier DY, Jungblut B. 2005. Genetic and cellular analyses of zebrafish atrioventricular cushion and valve development. Development 132:4193-4204.

Bharadwaj KN, Spitz C, Shekhar A, Yalcin HC, Butcher JT. 2012. Computational fluid dynamics of developing avian outflow tract heart valves. Ann Biomed Eng 40:2212-2227.

Boselli F, Freund JB, Vermot J. 2015. Blood flow mechanics in cardiovascular development. Cell Mol Life Sci 72:2545-2559.

Boselli F, Vermot J. 2016. Live imaging and modeling for shear stress quantification in the embryonic zebrafish heart. Methods 94:129-134.

Bournele D, Beis D. 2016. Zebrafish models of cardiovascular disease. Heart Failure Reviews:1-11.

Braddock M, Schwachtgen JL, Houston P, Dickson MC, Lee MJ, Campbell CJ. 1998. Fluid Shear Stress Modulation of Gene Expression in Endothelial Cells. News Physiol Sci 13:241-246.

Brown D, Samsa L, Qian L, Liu J. 2016. Advances in the Study of Heart Development and Disease Using Zebrafish. Journal of Cardiovascular Development and Disease 3:13.

Buskohl PR, Jenkins JT, Butcher JT. 2012. Computational simulation of hemodynamic-driven growth and remodeling of embryonic atrioventricular valves. Biomech Model Mechanobiol 11:1205-1217.

Butcher JT, Sedmera D, Guldberg RE, Markwald RR. 2007. Quantitative volumetric analysis of cardiac morphogenesis assessed through micro-computed tomography. Dev Dyn 236:802-809.

Caiazzo A, Guibert R, Boudjemline Y, Vignon-Clementel IE. 2015. Blood Flow Simulations for the Design of Stented Valve Reducer in Enlarged Ventricular Outflow Tracts. Cardiovasc Eng Technol 6:485-500.

Cammarato A, Ocorr S, Ocorr K. 2015. Enhanced assessment of contractile dynamics in Drosophila hearts. Biotechniques 58:77-80.

Chen JN, Haffter P, Odenthal J, Vogelsang E, Brand M, van Eeden FJ, Furutani-Seiki M, Granato M, Hammerschmidt M, Heisenberg CP, Jiang YJ, Kane DA, Kelsh RN, Mullins MC, Nusslein-Volhard C. 1996. Mutations affecting the cardiovascular system and other internal organs in zebrafish. Development 123:293-302.

Chi NC, Bussen M, Brand-Arzamendi K, Ding C, Olgin JE, Shaw RM, Martin GR, Stainier DY. 2010. Cardiac conduction is required to preserve cardiac chamber morphology. Proc Natl Acad Sci U S A 107:14662-14667.

Chico TJ, Ingham PW, Crossman DC. 2008. Modeling cardiovascular disease in the zebrafish. Trends Cardiovasc Med 18:150-155.

DeGroff CG. 2002. Doppler echocardiography. Pediatr Cardiol 23:307-333.

Denvir MA, Tucker CS, Mullins JJ. 2008. Systolic and diastolic ventricular function in zebrafish embryos: influence of norepenephrine, MS-222 and temperature. BMC Biotechnol 8:21.

Doost SN, Zhong L, Su B, Morsi YS. 2016. The numerical analysis of non-Newtonian blood flow in human patient-specific left ventricle. Comput Methods Programs Biomed 127:232-247.

Fahrbach FO, Voigt FF, Schmid B, Helmchen F, Huisken J. 2013. Rapid 3D light-sheet microscopy with a tunable lens. Optics Express 21:21010-21026.
Fink M, Callol-Massot C, Chu A, Ruiz-Lozano P, Izpisua Belmonte JC, Giles W, Bodmer R, Ocorr K. 2009. A new method for detection and quantification of heartbeat parameters in Drosophila, zebrafish, and embryonic mouse hearts. Biotechniques 46:101-113.
Garavito-Aguilar ZV, Riley HE, Yelon D. 2010. Hand2 ensures an appropriate environment for cardiac fusion by limiting Fibronectin function. Development 137:3215-3220.
Glickman NS, Yelon D. 2002. Cardiac development in zebrafish: coordination of form and function. Semin Cell Dev Biol 13:507-513.
Goetz Jacky G, Steed E, Ferreira Rita R, Roth S, Ramspacher C, Boselli F, Charvin G, Liebling M, Wyart C, Schwab Y, Vermot J. 2014. Endothelial Cilia Mediate Low Flow Sensing during Zebrafish Vascular Development. Cell Reports 6:799-808.
Goktas S, Chen CY, Kowalski WJ, Pekkan K. 2015. Hemodynamic flow visualization of early embryonic great vessels using muPIV. Methods Mol Biol 1189:17-30.
Gould RA, Yalcin HC, MacKay JL, Sauls K, Norris R, Kumar S, Butcher JT. 2016. Cyclic Mechanical Loading Is Essential for Rac1-Mediated Elongation and Remodeling of the Embryonic Mitral Valve. Curr Biol 26:27-37.
Haendchen RV, Wyatt HL, Maurer G, Zwehl W, Bear M, Meerbaum S, Corday E. 1983. Quantitation of regional cardiac function by two-dimensional echocardiography. I. Patterns of contraction in the normal left ventricle. Circulation 67:1234-1245.
Heckel E, Boselli F, Roth S, Krudewig A, Belting HG, Charvin G, Vermot J. 2015. Oscillatory Flow Modulates Mechanosensitive klf2a Expression through trpv4 and trpp2 during Heart Valve Development. Curr Biol 25:1354-1361.
Henning AL, Jiang MX, Yalcin HC, Butcher JT. 2011. Quantitative three-dimensional imaging of live avian embryonic morphogenesis via micro-computed tomography. Dev Dyn 240:1949-1957.
Hoage T, Ding Y, Xu X. 2012. Quantifying cardiac functions in embryonic and adult zebrafish. Methods Mol Biol 843:11-20.
Houk AR, Yelon D. 2016. Chapter 9 - Strategies for analyzing cardiac phenotypes in the zebrafish embryo. In: H. William Detrich MW, Leonard IZ, editors. Methods in Cell Biology. Academic Press. pp 335-368.
Hove JR. 2006. Quantifying cardiovascular flow dynamics during early development. Pediatr Res 60:6-13.
Hove JR, Craig MP. 2012. High-speed confocal imaging of zebrafish heart development. Methods Mol Biol 843:309-328.
Hove JR, Koster RW, Forouhar AS, Acevedo-Bolton G, Fraser SE, Gharib M. 2003. Intracardiac fluid forces are an essential epigenetic factor for embryonic cardiogenesis. Nature 421:172-177.
Hu N, Yost HJ, Clark EB. 2001. Cardiac morphology and blood pressure in the adult zebrafish. Anat Rec 264:1-12.
Huisken J, Stainier DY. 2009. Selective plane illumination microscopy techniques in developmental biology. Development 136:1963-1975.
Huisken J, Swoger J, Del Bene F, Wittbrodt J, Stelzer EHK. 2004. Optical Sectioning Deep Inside Live Embryos by Selective Plane Illumination Microscopy. Science 305:1007-1009.
Jamison RA, Samarage CR, Bryson-Richardson RJ, Fouras A. 2013. In Vivo Wall Shear Measurements within the Developing Zebrafish Heart. PLoS ONE 8:e75722.
Kalogirou S, Malissovas N, Moro E, Argenton F, Stainier DY, Beis D. 2014. Intracardiac flow dynamics regulate atrioventricular valve morphogenesis. Cardiovasc Res 104:49-60.
Kok FO, Shin M, Ni CW, Gupta A, Grosse AS, van Impel A, Kirchmaier BC, Peterson-Maduro J, Kourkoulis G, Male I, DeSantis DF, Sheppard-Tindell S, Ebarasi L, Betsholtz C, Schulte-Merker S, Wolfe SA,

Lawson ND. 2015. Reverse genetic screening reveals poor correlation between morpholino-induced and mutant phenotypes in zebrafish. Dev Cell 32:97-108.

Kuo CT, Morrisey EE, Anandappa R, Sigrist K, Lu MM, Parmacek MS, Soudais C, Leiden JM. 1997. GATA4 transcription factor is required for ventral morphogenesis and heart tube formation. Genes Dev 11:1048-1060.

Langille BL. 1995. Blood Flow-Induced Remodeling of the Artery Wall. In: Bevan JA, Kaley G, Rubanyi GM, editors. Flow-Dependent Regulation of Vascular Function. New York, NY: Springer New York. pp 277-299.

Lawson ND. 2016. Reverse Genetics in Zebrafish: Mutants, Morphants, and Moving Forward. Trends Cell Biol 26:77-79.

Lee J, Fei P, Packard RR, Kang H, Xu H, Baek KI, Jen N, Chen J, Yen H, Kuo CC, Chi NC, Ho CM, Li R, Hsiai TK. 2016a. 4-Dimensional light-sheet microscopy to elucidate shear stress modulation of cardiac trabeculation. J Clin Invest 126:1679-1690.

Lee J, Moghadam ME, Kung E, Cao H, Beebe T, Miller Y, Roman BL, Lien CL, Chi NC, Marsden AL, Hsiai TK. 2013. Moving domain computational fluid dynamics to interface with an embryonic model of cardiac morphogenesis. PLoS One 8:e72924.

Lee L, Genge CE, Cua M, Sheng X, Rayani K, Beg MF, Sarunic MV, Tibbits GF. 2016b. Functional Assessment of Cardiac Responses of Adult Zebrafish (Danio rerio) to Acute and Chronic Temperature Change Using High-Resolution Echocardiography. PLoS One 11:e0145163.

Li J, Cao Y, Wu Y, Chen W, Yuan Y, Ma X, Huang G. 2015. The expression profile analysis of NKX2-5 knock-out embryonic mice to explore the pathogenesis of congenital heart disease. J Cardiol 66:527-531.

Liebling M, Vermot J, Forouhar AS, Gharib M, Dickinson ME, Fraser SE. 2006. Nonuniform temporal alignment of slice sequences for four-dimensional imaging of cyclically deforming embryonic structures. In: 3rd IEEE International Symposium on Biomedical Imaging: Nano to Macro, 2006. pp 1156-1159.

Lieu DK, Pappone PA, Barakat AI. 2004. Differential membrane potential and ion current responses to different types of shear stress in vascular endothelial cells. Am J Physiol Cell Physiol 286:C1367-1375.

Lindsey SE, Butcher JT, Yalcin HC. 2014. Mechanical regulation of cardiac development. Frontiers in Physiology 5:318.

Lindsey SE, Menon PG, Kowalski WJ, Shekhar A, Yalcin HC, Nishimura N, Schaffer CB, Butcher JT, Pekkan K. 2015. Growth and hemodynamics after early embryonic aortic arch occlusion. Biomech Model Mechanobiol 14:735-751.

Liu J, Bressan M, Hassel D, Huisken J, Staudt D, Kikuchi K, Poss KD, Mikawa T, Stainier DY. 2010. A dual role for ErbB2 signaling in cardiac trabeculation. Development 137:3867-3875.

Liu Y, Asnani A, Zou L, Bentley VL, Yu M, Wang Y, Dellaire G, Sarkar KS, Dai M, Chen HH, Sosnovik DE, Shin JT, Haber DA, Berman JN, Chao W, Peterson RT. 2014. Visnagin protects against doxorubicin-induced cardiomyopathy through modulation of mitochondrial malate dehydrogenase. Sci Transl Med 6:266ra170.

Lu F, Langenbacher A, Chen J-N. 2016. Transcriptional Regulation of Heart Development in Zebrafish. Journal of Cardiovascular Development and Disease 3:14.

Mahou P, Vermot J, Beaurepaire E, Supatto W. 2014. Multicolor two-photon light-sheet microscopy. Nat Meth 11:600-601.

Martin RT, Bartman T. 2009. Analysis of heart valve development in larval zebrafish. Dev Dyn 238:1796-1802.

Mickoleit M, Schmid B, Weber M, Fahrbach FO, Hombach S, Reischauer S, Huisken J. 2014. High-resolution reconstruction of the beating zebrafish heart. Nat Meth 11:919-922.

Miller LA. 2011. Fluid dynamics of ventricular filling in the embryonic heart. Cell Biochem Biophys 61:33-45.
Nair N, Gerger C, Hatef A, Weber LP, Unniappan S. 2016. Ultrasonography reveals in vivo dose-dependent inhibition of end systolic and diastolic volumes, heart rate and cardiac output by nesfatin-1 in zebrafish. General and Comparative Endocrinology 234:142-150.
Nasevicius A, Ekker SC. 2000. Effective targeted gene 'knockdown' in zebrafish. Nat Genet 26:216-220.
Nguyen VT, Wibowo SN, Leow YA, Nguyen HH, Liang Z, Leo HL. 2015. A Patient-Specific Computational Fluid Dynamic Model for Hemodynamic Analysis of Left Ventricle Diastolic Dysfunctions. Cardiovasc Eng Technol 6:412-429.
Pelster B, Burggren WW. 1996. Disruption of hemoglobin oxygen transport does not impact oxygen-dependent physiological processes in developing embryos of zebra fish (Danio rerio). Circ Res 79:358-362.
Peshkovsky C, Totong R, Yelon D. 2011. Dependence of cardiac trabeculation on neuregulin signaling and blood flow in zebrafish. Dev Dyn 240:446-456.
Pestel J, Ramadass R, Gauvrit S, Helker C, Herzog W, Stainier DY. 2016. Real-time 3D visualization of cellular rearrangements during cardiac valve formation. 143:2217-2227.
Poelma C, Kloosterman A, Hierck BP, Westerweel J. 2012. Accurate Blood Flow Measurements: Are Artificial Tracers Necessary? PLoS ONE 7:e45247.
Poon KL, Brand T. 2013. The zebrafish model system in cardiovascular research: A tiny fish with mighty prospects. Global Cardiology Science & Practice 2013:9-28.
Rossi A, Kontarakis Z, Gerri C, Nolte H, Holper S, Kruger M, Stainier DYR. 2015. Genetic compensation induced by deleterious mutations but not gene knockdowns. Nature 524:230-233.
Samsa LA, Givens C, Tzima E, Stainier DY, Qian L, Liu J. 2015. Cardiac contraction activates endocardial Notch signaling to modulate chamber maturation in zebrafish. Development 142:4080-4091.
Samsa LA, Yang B, Liu J. 2013. Embryonic cardiac chamber maturation: Trabeculation, conduction, and cardiomyocyte proliferation. Am J Med Genet C Semin Med Genet 163c:157-168.
Scherz PJ, Huisken J, Sahai-Hernandez P, Stainier DY. 2008. High-speed imaging of developing heart valves reveals interplay of morphogenesis and function. Development 135:1179-1187.
Schulte-Merker S, Stainier DY. 2014. Out with the old, in with the new: reassessing morpholino knockdowns in light of genome editing technology. Development 141:3103-3104.
Shin JT, Pomerantsev EV, Mably JD, MacRae CA. 2010. High-resolution cardiovascular function confirms functional orthology of myocardial contractility pathways in zebrafish. Physiol Genomics 42:300-309.
Stainier DY. 2001. Zebrafish genetics and vertebrate heart formation. Nat Rev Genet 2:39-48.
Stainier DY, Fouquet B, Chen JN, Warren KS, Weinstein BM, Meiler SE, Mohideen MA, Neuhauss SC, Solnica-Krezel L, Schier AF, Zwartkruis F, Stemple DL, Malicki J, Driever W, Fishman MC. 1996. Mutations affecting the formation and function of the cardiovascular system in the zebrafish embryo. Development 123:285-292.
Stainier DY, Kontarakis Z, Rossi A. 2015. Making sense of anti-sense data. Dev Cell 32:7-8.
Steed E, Boselli F, Vermot J. 2016a. Hemodynamics driven cardiac valve morphogenesis. Biochim Biophys Acta 1863:1760-1766.
Steed E, Faggianelli N, Roth S, Ramspacher C, Concordet J-P, Vermot J. 2016b. klf2a couples mechanotransduction and zebrafish valve morphogenesis through fibronectin synthesis. Nature Communications 7:11646.
Ta-Shma A, Zhang K, Salimova E, Zernecke A, Sieiro-Mosti D, Stegner D, Furtado M, Shaag A, Perles Z, Nieswandt B, Rein AJ, Rosenthal N, Neiman AM, Elpeleg O. 2016. Congenital valvular defects associated with deleterious mutations in the PLD1 gene. J Med Genet.

Targoff KL, Colombo S, George V, Schell T, Kim SH, Solnica-Krezel L, Yelon D. 2013. Nkx genes are essential for maintenance of ventricular identity. Development 140:4203-4213.
Targoff KL, Schell T, Yelon D. 2008. Nkx genes regulate heart tube extension and exert differential effects on ventricular and atrial cell number. Dev Biol 322:314-321.
Taylor JM, Girkin JM, Love GD. 2012a. High-resolution 3D optical microscopy inside the beating zebrafish heart using prospective optical gating. Biomedical Optics Express 3:3043-3053.
Taylor JM, Saunter CD, Love GD, Girkin JM. 2012b. Prospective gating for 3D imaging of the beating zebrafish heart in embryonic development studies. In. pp 822716-822716-822717.
Tomer R, Khairy K, Keller PJ. 2011. Shedding light on the system: studying embryonic development with light sheet microscopy. Curr Opin Genet Dev 21:558-565.
Trinh LA, Yelon D, Stainier DY. 2005. Hand2 regulates epithelial formation during myocardial diferentiation. Curr Biol 15:441-446.
Trivedi V, Truong TV, Trinh le A, Holland DB, Liebling M, Fraser SE. 2015. Dynamic structure and protein expression of the live embryonic heart captured by 2-photon light sheet microscopy and retrospective registration. Biomed Opt Express 6:2056-2066.
Truong TV, Supatto W, Koos DS, Choi JM, Fraser SE. 2011. Deep and fast live imaging with two-photon scanned light-sheet microscopy. Nat Meth 8:757-760.
Vermot J, Forouhar AS, Liebling M, Wu D, Plummer D, Gharib M, Fraser SE. 2009. Reversing blood flows act through klf2a to ensure normal valvulogenesis in the developing heart. PLoS Biol 7:e1000246.
Wang LW, Huttner IG, Santiago CF, Kesteven SH, Yu ZY, Feneley MP, Fatkin D. 2016. Standardized echocardiographic assessment of cardiac function in normal adult zebrafish and heart disease models. Disease Models & Mechanisms.
Wang Y, Dur O, Patrick MJ, Tinney JP, Tobita K, Keller BB, Pekkan K. 2009. Aortic arch morphogenesis and flow modeling in the chick embryo. Ann Biomed Eng 37:1069-1081.
Weber M, Huisken J. 2011. Light sheet microscopy for real-time developmental biology. Current Opinion in Genetics & Development 21:566-572.
Weber M, Huisken J. 2015. In vivo imaging of cardiac development and function in zebrafish using light sheet microscopy. Swiss Med Wkly 145:w14227.
Weinstein BM, Stemple DL, Driever W, Fishman MC. 1995. gridlock, a localized heritable vascular patterning defect in the zebrafish. Nat Med 1:1143-1147.
White RM, Sessa A, Burke C, Bowman T, LeBlanc J, Ceol C, Bourque C, Dovey M, Goessling W, Burns CE, Zon LI. 2008. Transparent adult zebrafish as a tool for in vivo transplantation analysis. Cell Stem Cell 2:183-189.
Yalcin HC. 2014. Femtosecond laser photodisruption of vitelline vessels of avian embryos as a technique to study embryonic vascular remodeling. Exp Biol Med (Maywood) 239:1644-1652.
Yalcin HC, Shekhar A, McQuinn TC, Butcher JT. 2011. Hemodynamic patterning of the avian atrioventricular valve. Dev Dyn 240:23-35.
Yalcin HC, Shekhar A, Nishimura N, Rane AA, Schaffer CB, Butcher JT. 2010a. Two-photon microscopy-guided femtosecond-laser photoablation of avian cardiogenesis: noninvasive creation of localized heart defects. Am J Physiol Heart Circ Physiol 299:H1728-1735.
Yalcin HC, Shekhar A, Rane AA, Butcher JT. 2010b. An ex-ovo chicken embryo culture system suitable for imaging and microsurgery applications. J Vis Exp.

Figure Legends

Fig. 1. Heart development in zebrafish. **(A-C):** Lateral and dorsal views of heart development for different stage embryos. **D.** Cross sectional view of the heart at 3-5 dpf. Adapted from (Brown et al., 2016)

Fig. 2. Assessment of heart function via timelapse video microscopy in zebrafish. **A:** Brightfield image of a 3dpf transparent zebrafish embryo. Boxes designates the ventricle and dorsal aorta regions. B: M-mode imaging through short axis of the ventricle. D_d and D_s are diameters whereas MT_d and MT_s are myocardial thicknesses at diastole and systole. **C:** Individual RBCs can be traced for measuring blood flow velocity in the dorsal aorta region. **D:** Orientation of the ventricle and its schematic view. Arrows identifies a local myocardial wall thickness. Adapted from (Shin et al., 2010)

Fig. 3. Principles of Light Sheet Fluorescence Microscopy (LSFM). **A:** Schematic drawing illustrates orthogonal orientation of illumination (blue) and detection (green) beam paths. The sample is hold in a transparent gel and can be rotated around the central vertical axis. Light sheet illuminates the sample in the focal plane. Sample is moved through the light sheet to form an image stack which is then reconstructed for 3D geometry. Adapted from (Weber and Huisken, 2011). **B:** Comparison of LSFM with conventional point scanning confocal microscopy. Advantages of LSFM include high acquisition speed, high signal-to-noise ratio, minimal photo bleaching and high penetration depth. Adapted from (Huisken and Stainier, 2009)

Fig. 4. LSFM imaging of dynamic zebrafish hearts**. A:** 2D image of the atrioventricular canal for a 60 hpf embryo. Myocardial cells are labeled green and RBC in red in the image. A is atrium V is ventricle. Adapted from (Lee et al., 2016a). **B.** Top images are 3D rendering of a synchronized movie stack for atrium cut open for a 48 hpf embryo. Myocardial cells are labeled red and RBCs in green. Atrium is contracting from left to right images. Bottom images are tracking of RBCs for respective time points. Adapted from (Mickoleit et al., 2014; Weber and Huisken, 2015). **C.** Direct recording of a 4D movie for a beating zebrafish heart with improved image acquisition using a tunable lens. Adapted from (Fahrbach et al., 2013).

Fig. 5. Velocity and WSS measurements via DPIV for zebrafish embryos**. A:** Brightfield image for the ventricle of a 4 dpf zebrafish embryo. **B:** Vessel boundaries are determined as the limits of cell movements. **C:** Velocity vectors for cell movements**. D:** Calculated wall shear rates overlaid with velocity vectors. Adapted from (Jamison et al., 2013).

Fig. 6. Simplified mathematical model for 4.5 dpf zebrafish heart**. A:** Top sketch is the model with rigid walls and bottom sketch is the model with elastic atrial and ventricular walls. In the deformable model, contraction of the ventricle fills the ventricle. d is the diameter of the channel, c is the depth of the chambers, a is atrium, v is ventricle. **B**: Velocity streamlines in the rigid (top) and flexible (bottom) wall models. Flexible models captures streamline behavior better. **C:** WSS levels in dynes/cm^2 for the rigid (top) and flexible (bottom) wall models. WSS estimations for the flexible model looks more realistic. Adapted from (Miller, 2011).

Fig. 7. Moving domain computational models for zebrafish hearts. **A:** The use of transgenic Tg(fli1a:EGFP)y1 embryos allows for clear identification of inner wall for reconstructing the CFD model geometry. A is atria, V is ventricle, B is bulbus arteriosus. **B:** Computationally determined velocity levels at AV canal at peak systole for different stage embryos. High gradients are localized to valve region indicating high WSS. **C:** Averaged peak flow WSS and pressure gradient at AV canal for different stage embryos. Both values increase significantly throughout development. **D:** Velocity streamline patterns at atrial relaxation, demonstrates varying vortex characteristics for different stages. Adapted from (Lee et al., 2013).

Fig. 8. Coupled confocal imaging and computational modeling approach for zebrafish heart hemodynamics**. A:** Segmentation of the heart wall from maximum intensity projection of a confocal scan for a 48 hpf embryo. **B:** Cross-section segments through the heart and their intersection points with the wall. ATR is atrium, VNT is ventricle, AVC is atrioventricular canal. **C:** Velocity vectors and WSS levels from the in-silico CFD model at peak systole. Adapted from (Boselli and Vermot, 2016)

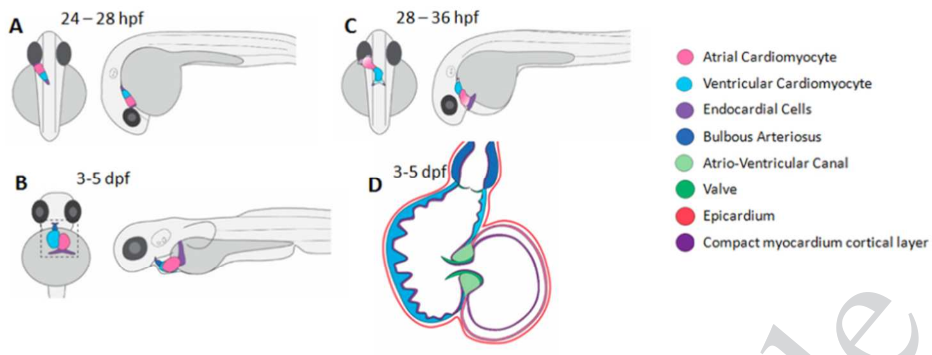

Fig. 1. Heart development in zebrafish. (A-C): Lateral and dorsal views of heart development for different stage embryos. D. Cross sectional view of the heart at 3-5 dpf. Adapted from (Brown et al., 2016)

85x30mm (300 x 300 DPI)

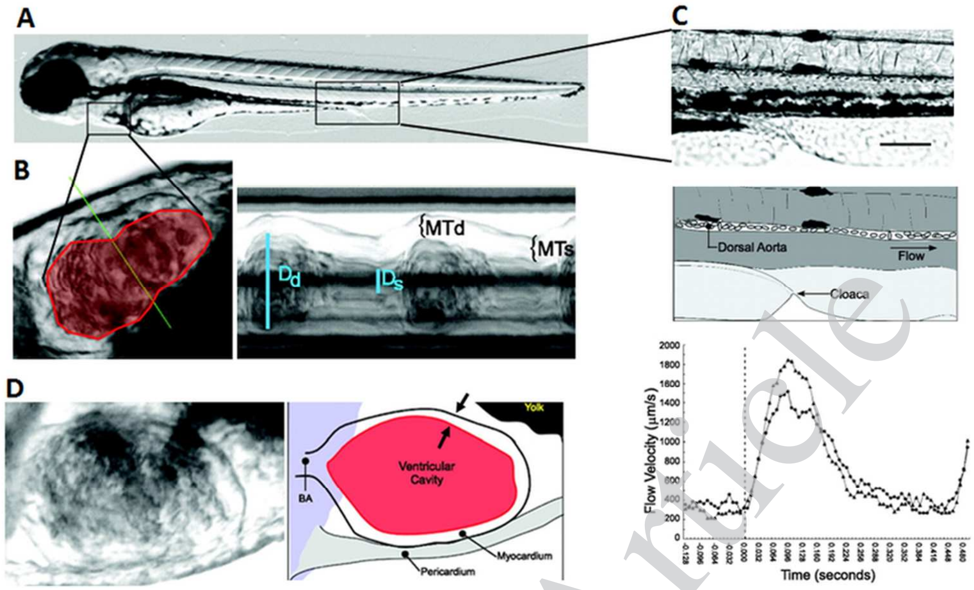

Fig. 2. Assessment of heart function via timelapse video microscopy in zebrafish. A: Brightfield image of a 3dpf transparent zebrafish embryo. Boxes designates the ventricle and dorsal aorta regions. B: M-mode imaging through short axis of the ventricle. Dd and Ds are diameters whereas MTd and MTs are myocardial thicknesses at diastole and systole. C: Individual RBCs can be traced for measuring blood flow velocity in the dorsal aorta region. D: Orientation of the ventricle and its schematic view. Arrows identifies a local myocardial wall thickness. Adapted from (Shin et al., 2010)

85x51mm (300 x 300 DPI)

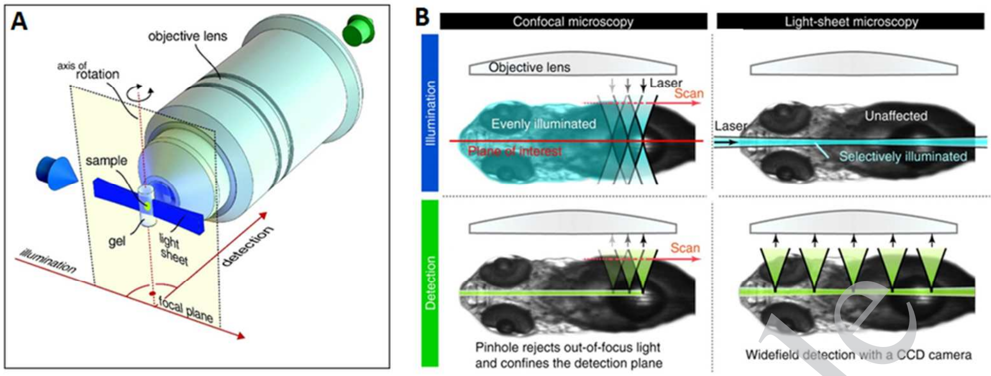

Fig. 3. Principles of Light Sheet Fluorescence Microscopy (LSFM). A: Schematic drawing illustrates orthogonal orientation of illumination (blue) and detection (green) beam paths. The sample is hold in a transparent gel and can be rotated around the central vertical axis. Light sheet illuminates the sample in the focal plane. Sample is moved through the light sheet to form an image stack which is then reconstructed for 3D geometry. Adapted from (Weber and Huisken, 2011). B: Comparison of LSFM with conventional point scanning confocal microscopy. Advantages of LSFM include high acquisition speed, high signal-to-noise ratio, minimal photo bleaching and high penetration depth. Adapted from (Huisken and Stainier, 2009)

85x41mm (300 x 300 DPI)

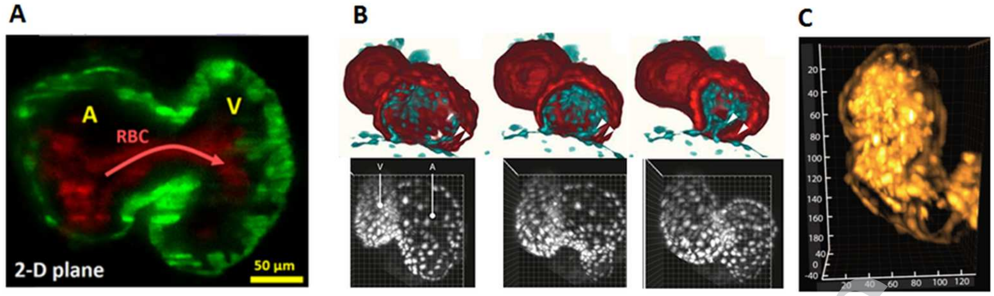

Fig. 4. LSFM imaging of dynamic zebrafish hearts. A: 2D image of the atrioventricular canal for a 60 hpf embryo. Myocardial cells are labeled green and RBC in red in the image. A is atrium V is ventricle. Adapted from (Lee et al., 2016a). B. Top images are 3D rendering of a synchronized movie stack for atrium cut open for a 48 hpf embryo. Myocardial cells are labeled red and RBCs in green. Atrium is contracting from left to right images. Bottom images are tracking of RBCs for respective time points. Adapted from (Mickoleit et al., 2014; Weber and Huisken, 2015). C. Direct recording of a 4D movie for a beating zebrafish heart with improved image acquisition using a tunable lens. Adapted from (Fahrbach et al., 2013).

85x26mm (300 x 300 DPI)

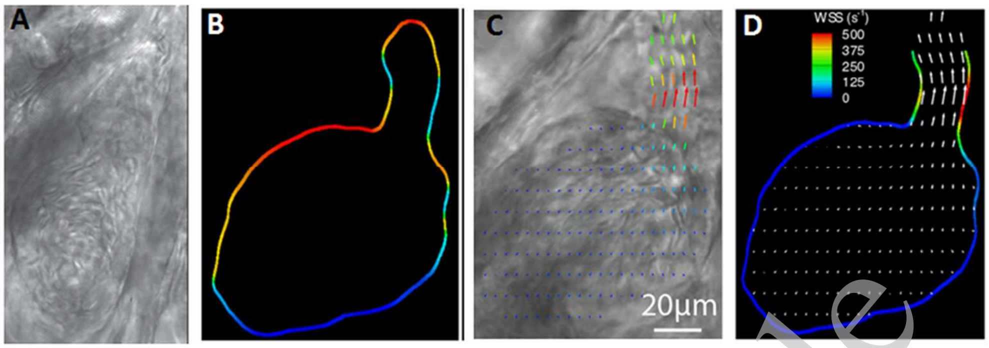

Fig. 5. Velocity and WSS measurements via DPIV for zebrafish embryos. A: Brightfield image for the ventricle of a 4 dpf zebrafish embryo. B: Vessel boundaries are determined as the limits of cell movements. C: Velocity vectors for cell movements. D: Calculated wall shear rates overlaid with velocity vectors. Adapted from (Jamison et al., 2013).

85x30mm (300 x 300 DPI)

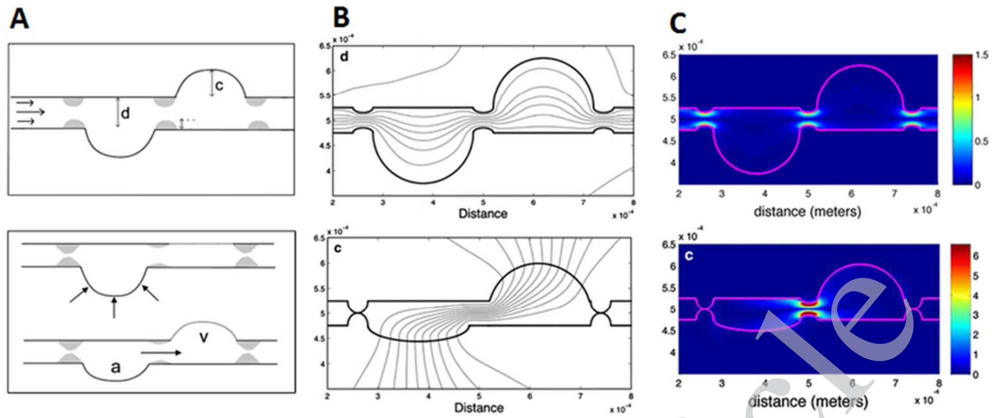

Fig. 6. Simplified mathematical model for 4.5 dpf zebrafish heart. A: Top sketch is the model with rigid walls and bottom sketch is the model with elastic atrial and ventricular walls. In the deformable model, contraction of the ventricle fills the ventricle. d is the diameter of the channel, c is the depth of the chambers, a is atrium, v is ventricle. B: Velocity streamlines in the rigid (top) and flexible (bottom) wall models. Flexible models captures streamline behavior better. C: WSS levels in dynes/cm2 for the rigid (top) and flexible (bottom) wall models. WSS estimations for the flexible model looks more realistic. Adapted from (Miller, 2011).

85x36mm (300 x 300 DPI)

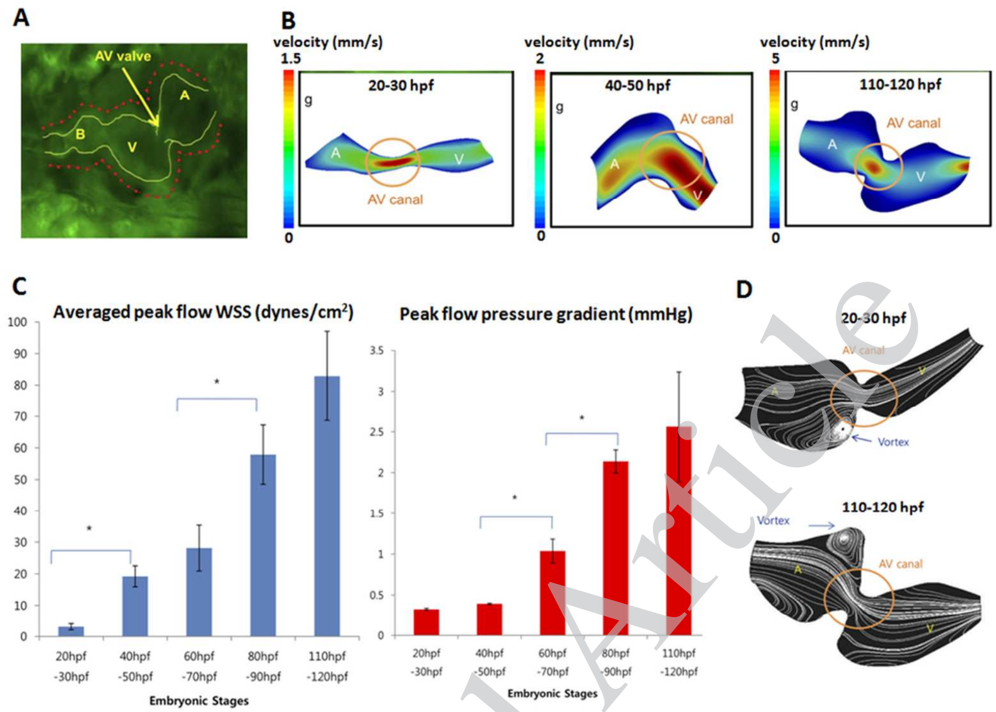

Fig. 7. Moving domain computational models for zebrafish hearts. A: The use of transgenic Tg(fli1a:EGFP)y1 embryos allows for clear identification of inner wall for reconstructing the CFD model geometry. A is atria, V is ventricle, B is bulbus arteriosus. B: Computationally determined velocity levels at AV canal at peak systole for different stage embryos. High gradients are localized to valve region indicating high WSS. C: Averaged peak flow WSS and pressure gradient at AV canal for different stage embryos. Both values increase significantly throughout development. D: Velocity streamline patterns at atrial relaxation, demonstrates varying vortex characteristics for different stages. Adapted from (Lee et al., 2013).

85x61mm (300 x 300 DPI)

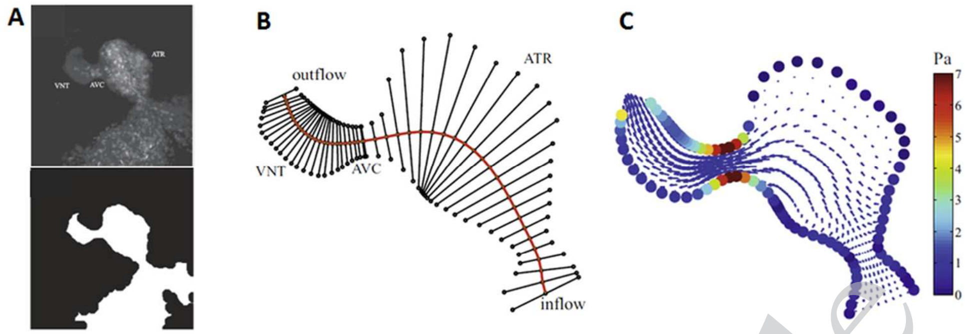

Fig. 8. Coupled confocal imaging and computational modeling approach for zebrafish heart hemodynamics. A: Segmentation of the heart wall from maximum intensity projection of a confocal scan for a 48 hpf embryo. B: Cross-section segments through the heart and their intersection points with the wall. ATR is atrium, VNT is ventricle, AVC is atrioventricular canal. C: Velocity vectors and WSS levels from the in-silico CFD model at peak systole. Adapted from (Boselli and Vermot, 2016)

85x29mm (300 x 300 DPI)